

Confinement efficiency and size effect of FRP confined circular concrete columns

Fang-Yao Yeh[†]

Photovoltaic Technology Center, Industrial Technology Research Institute, Taiwan, 310, R.O.C.

Kuo-Chun Chang[‡]

Department of Civil Engineering, National Taiwan University, Taipei, Taiwan, 10617, R.O.C.

(Received November 21, 2005, Accepted November 10, 2006)

Abstract. The objective of this paper is to develop a finite element procedure for predicting the compressive strength and ultimate axial strain of Carbon Fiber Reinforced Plastics (CFRP) confined circular concrete columns and to study the effective parameters of confinement efficiency for helping design of CFRP retrofit technology. The behavior of concrete confined with CFRP is studied using the nonlinear finite element method. In this paper, effects of column size, CFRP volumetric ratio and plain concrete strength are studied. The confined concrete nonlinear constitutive relation, concrete failure criterion and stiffness reduction methodology after concrete cracking or crushing are adopted. First, the finite element model is verified by comparing the numerical solutions of confined concrete with experimental results. Then the effects of column size, CFRP volumetric ratio and plain concrete strength on the peak strength and ductility of the confined concrete are considered. The results of parametric study indicate that the normalized column axial strength increases with increasing CFRP volumetric ratio, but without size effect for columns with the same CFRP volumetric ratio. As the same, the increase in column ductility depends on CFRP volumetric ratio but without size effect for columns with the same CFRP volumetric ratio.

Keywords: FRP; strength of confined concrete; ductility; confinement efficiency; size effect.

1. Introduction

Steel jacketing has proved to be an effective measure for retrofitting reinforced concrete member and has been widely used in practice, but the engineering community is still looking for alternatives. Recently, the use of advanced composite materials, especially Fiber Reinforced Polymers (FRP), has been recognized as a reliable retrofit technique for reinforced concrete elements.

External confinement by FRP jackets is now a popular method for the retrofitting of Reinforced Concrete (RC) columns. To predict the strength and ductility of these columns subjected to combined bending and compression, an accurate stress-strain model is required for the FRP-confined concrete in the column. Many stress-strain models have been proposed for FRP-confined

[†] Manager and Researcher, E-mail: fyeh@itri.org.tw

[‡] Professor, Corresponding author, E-mail: ciekuo@ntu.edu.tw

concrete, but there is still a lack of consensus as to which model is the most suitable for use in the prediction of column strength and ductility.

In order to consider the effect of column diameters and some other parameters, a nonlinear finite element model is proposed for confined concrete in this paper. The aim of this paper is to compare the effects of column size, FRP volumetric ratio and plain concrete strength on the strength and ductility of confined concrete using the nonlinear finite element method.

2. Confined concrete model

2.1 Steel based constitutive model

Lateral confinement has been proven to enhance the mechanical properties of concrete members. The performance of the member depends upon the interaction of the confined concrete and the confining material. The success of lateral confinement is due to the development of triaxial stress field within the confined concrete and the containment of concrete after its disintegration. There are many stress-strain models that can be used in the steel confined concrete. One of the most widely used models for confined concrete was proposed by Mander *et al.* (1988). A comparison of existing stress-strain models for steel confined concrete has been conducted by Hoshikuma *et al.* (1997).

2.2 FRP based constitutive model

A number of stress-strain models are available for FRP-confined concrete listed in Table 1 (e.g., Fardis and Khalili 1982, Karbhari and Gao 1997, Kawashima *et al.* 1997, Samaan *et al.* 1998, Miyauchi *et al.* 1999, Saafi *et al.* 1999, Spoelstra and Monti 1999, Toutangi *et al.* 1999, Xiao and

Table 1 Summary of previous stress-strain models for FRP confined concrete

Researcher	Stress-strain model for FRP confined concrete		Applicable cross-sectional shape
	Ascending branch	Descending branch	
Fardis and Khalili (1982)	$\sigma = \frac{E_c \varepsilon}{1 + \varepsilon \left(\frac{\sigma_u}{E_u} - \frac{1}{\varepsilon_u} \right)}$		circle
Karbhari and Gao (1997)	$\sigma_A = f_{co}' + 4.1 f_{co}' v_c \frac{2t E_{com}}{d E_c}$ $\varepsilon^A = \frac{\sigma_A}{E^{eff}}$		circle
	$0 \leq \varepsilon_c \leq \varepsilon_t$	$\varepsilon_t \leq \varepsilon_c \leq \varepsilon_{cu}$	
Kawashima <i>et al.</i> (1998)	$f_c = E_c \varepsilon_c \left\{ 1 - \frac{1}{n} \left(\frac{\varepsilon_c}{\varepsilon_t} \right)^{n-1} \right\}$ for $E_g \leq 0$ $f_c = E_c \varepsilon_c \left\{ 1 - \frac{1}{n} \left(1 - \frac{E_g}{E_c} \right) \left(\frac{\varepsilon_c}{\varepsilon_t} \right)^{n-1} \right\}$ for $E_g \geq 0$	$f_c = f_t + E_g (\varepsilon_c - \varepsilon_t)$	circle square

Table 1 Continued

Researcher	Stress-strain model for FRP confined concrete		Applicable cross-sectional shape
	Ascending branch	Descending branch	
Samaan <i>et al.</i> (1998)	$f_c = \frac{(E_1 - E_2) \varepsilon_c}{\left[1 + \left(\frac{(E_1 - E_2) \varepsilon_c}{f_o}\right)^{n-1/n}\right]} + E_2 \varepsilon_c$		circle
Miyauchi <i>et al.</i> (1999)	<p>1. For the increasing type</p> $f_c = f_o \{2(\varepsilon_c / \varepsilon_o) - (\varepsilon_c / \varepsilon_o)^2\}$ for $0 \leq \varepsilon_c \leq \varepsilon_{tan}$ $f_c = f_{cu} - \lambda(\varepsilon_{cu} - \varepsilon_c)$ for $\varepsilon_{tan} \leq \varepsilon_c \leq \varepsilon_u$ <p>2. For the decreasing type</p> $f_c = f_o \{2(\varepsilon_c / \varepsilon_o) - (\varepsilon_c / \varepsilon_o)^2\}$ for $0 \leq \varepsilon_c \leq \varepsilon_o$	<p>For $\varepsilon_o \leq \varepsilon_c \leq \varepsilon_{cu}$</p> $f_c = f_o + (\varepsilon_c - \varepsilon_o) \frac{f_{cu} - f_o}{\varepsilon_{cu} - \varepsilon_o}$	circle
Toutanji (1999)	<p>1. $0 \leq \varepsilon \leq \varepsilon_1$</p> $f_a = \frac{E_{ii} \varepsilon_i}{1 + \left(\frac{E_{ii}}{f_{ua}} - \frac{2}{\varepsilon_{ui}} + \frac{E_{ui} E_{ii} \varepsilon_{ui}}{f_{ua}^2}\right) \varepsilon_i + \left(\frac{1}{\varepsilon_{ui}^2} - \frac{E_{ui} E_{ii}}{f_{ua}^2}\right) \varepsilon_i^2}$ <p>2. $\varepsilon_1 \leq \varepsilon \leq \varepsilon_{cu}$</p> $f_a = f_c' \left[1 + 3.5 \left(\frac{f_i}{f_c'}\right)^{0.85}\right]$		circle
Saafi <i>et al.</i> (1999)	<p>1. $0 \leq \varepsilon \leq \varepsilon_1$</p> $f = \frac{E_1 \varepsilon}{1 + \left(\frac{E_1}{f_a} - \frac{2}{\varepsilon_1} + \frac{E_2 E_1 \varepsilon_1}{f_a^2}\right) \varepsilon + \left(\frac{1}{\varepsilon_1^2} - \frac{E_1 E_2}{f_a^2}\right) \varepsilon^2}$ <p>2. $\varepsilon_1 \leq \varepsilon \leq \varepsilon_{cu}$</p> $f(\varepsilon_i) = f_c' \left(1 + 2.2 \left(\frac{f_i}{f_c'}\right)^{0.84}\right)$		circle
Xiao and Wu (2000)	<p>1. $0 \leq f_{cz} \leq f_c'$</p> $f_{cz} = E_c \varepsilon_{cz} + 2 \nu_c f_r$ $\varepsilon_r = -\frac{\nu_c}{1 + \frac{C_j}{E_c} (1 - \nu_c - 2 \nu_c^2)} \varepsilon_z; f_r = -C_j \varepsilon_r$ <p>2. $f_{cz} > f_c'$</p> $f_{cz} = 1.1 f_c' + \left(4.1 - 0.75 \frac{f_c'^2}{C_j}\right) f_r$ $\varepsilon_r = \varepsilon_{r0}' - \nu_c' \varepsilon_{cz}; f_r = -C_j \varepsilon_r$	$f_{cz} = \alpha f_c' + k f_r$ $\varepsilon_r = \varepsilon_{r0}' - \nu_c' \varepsilon_{cz}$ $f_r = -C_j \varepsilon_r$	circle
Li <i>et al.</i> (2003)	<p>$0 \leq \varepsilon_c \leq \varepsilon_{cc}'$</p> $f_c = f_{cc}' \left[-\left(\frac{\varepsilon_c}{\varepsilon_{cc}'}\right)^2 + 2\left(\frac{\varepsilon_c}{\varepsilon_{cc}'}\right)\right]$	<p>$\varepsilon_{cc}' \leq \varepsilon_c \leq \varepsilon_u$</p> $f_c = f_{cc}' - E_{des} (\varepsilon_c - \varepsilon_{cc}')$	circle

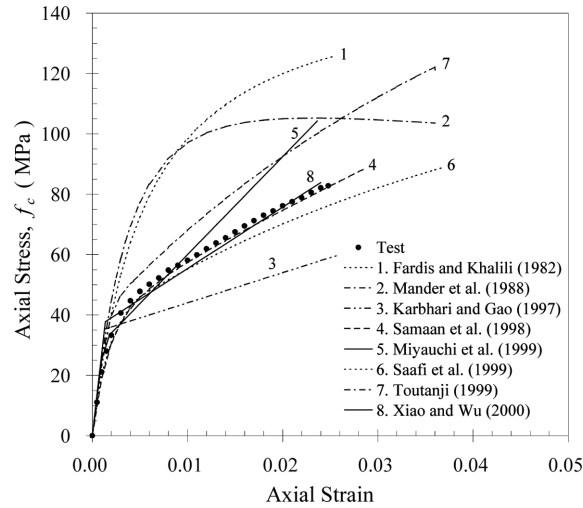


Fig. 1 Comparison of different stress-strain models for FRP confined concrete (Yuan *et al.* 2001)

Wu 2000, Li *et al.* 2003). A comparison of existing stress-strain models for FRP-confined concrete with test data of axially loaded FRP-confined circular concrete specimens has been conducted by Yuan *et al.* (2001), except for the stress-strain model of Spoelstra and Monti (1999), which requires an iterative procedure to generate stress-strain curves. Fig. 1 shows different theoretical stress-strain curves together with an experimental stress-strain curve obtained by Xiao and Wu (2000). It is clear from Fig. 1 that there exist large differences among different stress-strain models.

It should be noted that while most of the available stress-strain models for FRP-confined concrete are for monotonically ascending stress-strain curves only, a few of them (Kawashima *et al.* 1997, Miyachi *et al.* 1999, Spoelstra and Monti 1999, Xiao and Wu 2000, Li *et al.* 2003) include the possibility of a descending branch after the stress-strain curve peaks at f'_{cc} , with the ultimate axial strain ϵ_{cu} being greater than the axial strain ϵ_{cc} at peak stress.

3. FRP confined concrete nonlinear finite element model

A FRP jacket, as opposed to a steel one that applies a constant confining pressure after yield, has an elastic behavior up to failure and therefore exerts a continuously increasing confining action. The amount of this action depends on the lateral dilation of concrete, which in turn is affected by the confining pressure. As the compressive stress on the concrete increases, it begins to crack internally and expand laterally, resulting in an apparent increase in Poisson's ratio. The confinement effect is sensitive to the Poisson's ratio of concrete. The Poisson's ratio of concrete is not a constant. In this paper, the Poisson's ratio effect introduced by Kupfer *et al.* (1969) is followed that allow one to implicitly account for the lateral dilation of concrete and its interaction with the FRP jacket. The Poisson's ratio can be expressed in the form

$$\nu = \nu_0 \left[1.0 + 1.3763 \frac{\epsilon_c}{\epsilon_{c0}} - 5.36 \left(\frac{\epsilon_c}{\epsilon_{c0}} \right)^2 + 8.586 \left(\frac{\epsilon_c}{\epsilon_{c0}} \right)^3 \right] \quad (1)$$

where ϵ_c = strain in direction of uniaxial loading; ϵ_{c0} = compressive strain of unconfined concrete

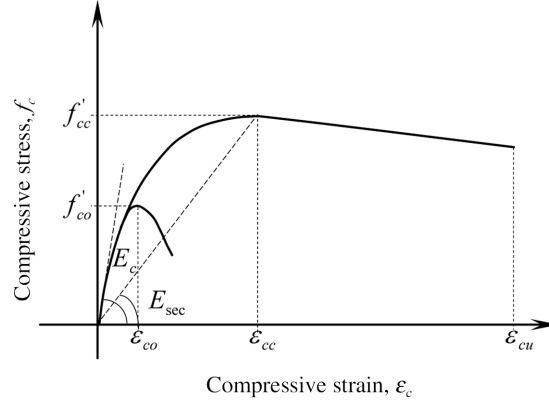


Fig. 2 Confined concrete model proposed by Mander

peak stress, respectively (generally $\varepsilon_{co} = 0.002$ can be assumed); $\nu_0 = 0.2$, the initial value of ν .

The nonlinear finite element model, including nonlinear constitutive relation, concrete failure criterion and stiffness reduction methodology after concrete cracking or crushing, is developed as follows.

3.1 Nonlinear constitutive relation

The starting point is a well-known stress-strain model for confined concrete (Mander *et al.* 1988, Fig. 2), which has been extensively tested against experimental data. The model is based on the formula (Popovics 1973)

$$f_c = \frac{f'_{cc} x r}{r - 1 + x^r} \quad (2)$$

where

$$x = \frac{\varepsilon_c}{\varepsilon_{cc}}, \quad \varepsilon_{cc} = \varepsilon_{co} \left[1 + 5 \left(\frac{f'_{cc}}{f'_{co}} - 1 \right) \right] \quad (3a,b)$$

$$r = \frac{E_c}{E_c - E_{sec}}; \quad E_{sec} = \frac{f'_{cc}}{\varepsilon_{cc}} \quad (4a,b)$$

where f'_{cc} = compressive strength of confined concrete; f'_{co} = compressive strength of unconfined concrete; ε_{cc} = compressive strain at confined peak stress f'_{cc} ; E_c = Young's modulus for concrete.

The confined concrete compressive strength f'_{cc} is expressed in terms of equal effective lateral confining pressure f'_l as follows

$$f'_{cc} = f'_{co} \left(-1.254 + 2.254 \sqrt{1 + \frac{7.94 f'_l}{f'_{co}}} - 2 \frac{f'_l}{f'_{co}} \right) \quad (5)$$

3.2 Element stress-strain relationship

Concrete element is used for the three-dimensional modeling of solids with or without reinforcing rebars. The solid is capable of cracking in tension and crushing in compression. The stress-strain

matrix $[D]_{RC}$ used for this element is defined as

$$[D]_{RC} = \left(1 - \sum_{i=1}^{N_r} V_i^R \right) [D_c] + \sum_{i=1}^{N_r} V_i^R [D_r]_i \quad (6)$$

where N_r = number of reinforcing materials; V_i^R = ratio of the volume of reinforcing material i to the total volume of the element; $[D_c]$ = stress-strain matrix for concrete, define by Eq. (7); and $[D_r]_i$ = stress-strain matrix for reinforcement i , defined by Eq. (8).

The matrix $[D_c]$ is defined as

$$[D_c] = \frac{E_c}{(1 + \nu)(1 - 2\nu)} \begin{bmatrix} (1 - \nu) & \nu & \nu & 0 & 0 & 0 \\ \nu & (1 - \nu) & \nu & 0 & 0 & 0 \\ \nu & \nu & (1 - \nu) & 0 & 0 & 0 \\ 0 & 0 & 0 & \frac{(1 - 2\nu)}{2} & 0 & 0 \\ 0 & 0 & 0 & 0 & \frac{(1 - 2\nu)}{2} & 0 \\ 0 & 0 & 0 & 0 & 0 & \frac{(1 - 2\nu)}{2} \end{bmatrix} \quad (7)$$

where E_c = Young's modulus for concrete; ν = Poisson's ratio for concrete.

The stress-strain matrix $[D_r]_i$ with respect to each coordinate system (x_i^r, y_i^r, z_i^r) has the form

$$\begin{Bmatrix} \sigma_{xx}^r \\ \sigma_{yy}^r \\ \sigma_{zz}^r \\ \sigma_{xy}^r \\ \sigma_{yz}^r \\ \sigma_{xz}^r \end{Bmatrix} = \begin{bmatrix} E_i^r & 0 & 0 & 0 & 0 & 0 \\ 0 & 0 & 0 & 0 & 0 & 0 \\ 0 & 0 & 0 & 0 & 0 & 0 \\ 0 & 0 & 0 & 0 & 0 & 0 \\ 0 & 0 & 0 & 0 & 0 & 0 \\ 0 & 0 & 0 & 0 & 0 & 0 \end{bmatrix} \begin{Bmatrix} \varepsilon_{xx}^r \\ \varepsilon_{yy}^r \\ \varepsilon_{zz}^r \\ \varepsilon_{xy}^r \\ \varepsilon_{yz}^r \\ \varepsilon_{xz}^r \end{Bmatrix} = [D_r]_i \begin{Bmatrix} \varepsilon_{xx}^r \\ \varepsilon_{yy}^r \\ \varepsilon_{zz}^r \\ \varepsilon_{xy}^r \\ \varepsilon_{yz}^r \\ \varepsilon_{xz}^r \end{Bmatrix} \quad (8)$$

where E_i^r = Young's modulus of reinforcement type i .

The CFRP jacket is model by thin shell elements. The stress-strain matrix $[D]_{cf}$ used for composite material in j -layer of the three-dimensional shell element is define as (Yunus and Kohnke 1989)

$$[D]_{cf} = \begin{bmatrix} BE_{x,j} & B\nu_{xy,j}E_{x,j} & 0 & 0 & 0 & 0 \\ B\nu_{xy,j}E_{x,j} & BE_{y,j} & 0 & 0 & 0 & 0 \\ 0 & 0 & 0 & 0 & 0 & 0 \\ 0 & 0 & 0 & G_{xy,j} & 0 & 0 \\ 0 & 0 & 0 & 0 & \frac{G_{yz,j}}{f} & 0 \\ 0 & 0 & 0 & 0 & 0 & \frac{G_{yz,j}}{f} \end{bmatrix} \quad (9)$$

where

$$B = \frac{E_{y,j}}{E_{y,j} - (\nu_{xy,j})^2 E_{x,j}}; \quad f = \text{Max} \left\{ \begin{array}{l} 1.2 \\ 1.0 + 0.2 \frac{A}{25t^2} \end{array} \right\} \quad (10a,b)$$

where $E_{x,j}$ = Young's modulus in layer x direction of layer j ; $E_{y,j}$ = Young's modulus in layer y direction of layer j ; $\nu_{xy,j}$ = Poisson's ratio in layer x - y plane of layer j ; $G_{xy,j}$ = shear modulus in layer x - y plane of layer j ; $G_{yz,j}$ = shear modulus in layer y - z plane of layer j ; $G_{xz,j}$ = shear modulus in layer x - z plane of layer j ; A = area of element in layer plane; t = average thickness of shell element.

3.3 Failure criterion

The failure criterion of concrete due to a multi-axial stress state can be expressed in the form

$$\frac{F}{f'_{co}} - S \geq 0 \quad (11)$$

where F = a function of the principal stress state; S = failure surface; and f'_{co} = uniaxial compressive strength.

In the compression-compression-compression region ($0 \geq \sigma_1 \geq \sigma_2 \geq \sigma_3$), the failure criterion of Willam and Warnke (1975) is implemented. In this case, F takes the form

$$F = F_1 = \frac{1}{\sqrt{15}} [(\sigma_1 - \sigma_2)^2 + (\sigma_2 - \sigma_3)^2 + (\sigma_3 - \sigma_1)^2]^{1/2} \quad (12)$$

and S is defined as

$$S = S_1 = \frac{2r_2(r_2^2 - r_1^2)\cos\eta + r_2(2r_1 - r_2)[4(r_2^2 - r_1^2)\cos^2\eta + 5r_1^2 - 4r_1r_2]^{1/2}}{4(r_2^2 - r_1^2)\cos^2\eta + (r_2 - 2r_1)^2} \quad (13)$$

The terms used to define S are

$$\cos\eta = \frac{2\sigma_1 - \sigma_2 - \sigma_3}{\sqrt{2}[(\sigma_1 - \sigma_2)^2 + (\sigma_2 - \sigma_3)^2 + (\sigma_3 - \sigma_1)^2]^{1/2}} \quad (14)$$

$$r_1 = a_0 + a_1\xi + a_2\xi^2 \quad (15)$$

$$r_2 = b_0 + b_1\xi + b_2\xi^2 \quad (16)$$

$$\xi = \frac{\sigma_h}{f'_{co}}, \quad \sigma_h = \frac{1}{3}(\sigma_1 + \sigma_2 + \sigma_3) \quad (17a,b)$$

If the failure criterion is satisfied in directions 1, 2 and 3, cracking occurs in the planes perpendicular to principal stresses σ_1 , σ_2 , and σ_3 . If the failure criterion is satisfied in directions 1 and 2, cracking occurs in the planes perpendicular to principal stresses σ_1 and σ_2 . If the failure criterion is satisfied only in direction 1, cracking occurs in the plane perpendicular to principal stress σ_1 .

In this paper, Tsai-Wu failure criterion is proposed to use in composite materials. Tsai and Hahn introduced the strength index failure criterion in 1980 and then Tsai introduced another strength ratio failure criterion in 1987, they can be expressed in this form

For strength index failure criterion

$$\zeta = A + B \quad (18)$$

For strength ratio failure criterion

$$\zeta = \frac{1.0}{\left(-\frac{B}{2A} + \sqrt{(B/2A)^2 + 1.0/A}\right)} \quad (19)$$

where ζ = the discriminant of Tsai-Wu failure criterion and

$$A = -\frac{(\sigma_x)^2}{\sigma_{xt}^f \sigma_{xc}^f} - \frac{(\sigma_y)^2}{\sigma_{yt}^f \sigma_{yc}^f} - \frac{(\sigma_z)^2}{\sigma_{zt}^f \sigma_{zc}^f} + \frac{(\sigma_{xy})^2}{(\sigma_{xy}^f)^2} + \frac{(\sigma_{yz})^2}{(\sigma_{yz}^f)^2} + \frac{(\sigma_{xz})^2}{(\sigma_{xz}^f)^2} \\ + \frac{C_{xy} \sigma_x \sigma_y}{\sqrt{\sigma_{xt}^f \sigma_{xc}^f \sigma_{yt}^f \sigma_{yc}^f}} + \frac{C_{yz} \sigma_y \sigma_z}{\sqrt{\sigma_{yt}^f \sigma_{yc}^f \sigma_{zt}^f \sigma_{zc}^f}} + \frac{C_{xz} \sigma_x \sigma_z}{\sqrt{\sigma_{xt}^f \sigma_{xc}^f \sigma_{zt}^f \sigma_{zc}^f}} \quad (20)$$

$$B = \left(\frac{1}{\sigma_{xt}^f} + \frac{1}{\sigma_{xc}^f}\right) \sigma_x + \left(\frac{1}{\sigma_{yt}^f} + \frac{1}{\sigma_{yc}^f}\right) \sigma_y + \left(\frac{1}{\sigma_{zt}^f} + \frac{1}{\sigma_{zc}^f}\right) \sigma_z \quad (21)$$

where C_{xy}, C_{yz}, C_{xz} = coefficients of Tsai-Wu failure theory considered stress coupling effect in $x-y$, $y-z$ and $x-z$ directions.

3.4 Stiffness reduction methodology

In this paper, the finite element concrete model predicts either elastic behavior, cracking behavior or crushing behavior. If elastic behavior is predicted, the concrete is treated as a linear elastic material. If cracking or crushing behavior is predicted, the elastic, stress-strain matrix is adjusted as discussed below for each failure mode.

The presence of a crack at an integration point is represented through modification of the stress-strain relation by introducing a plane of weakness in a direction normal to the crack face. Also, a shear transfer coefficient β_i is introduced which represents a shear strength reduction factor for those subsequent loads which induce sliding across the crack face. The stress-strain relations for a material that has cracked in one direction only become

$$[D_c^{ck}] = \frac{E_c}{(1+\nu)(1-2\nu)} \begin{bmatrix} 0 & 0 & 0 & 0 & 0 & 0 \\ 0 & \frac{1-2\nu}{1-\nu} & \frac{\nu(1-2\nu)}{1-\nu} & 0 & 0 & 0 \\ 0 & \frac{\nu(1-2\nu)}{1-\nu} & \frac{1-2\nu}{1-\nu} & 0 & 0 & 0 \\ 0 & 0 & 0 & \beta_i \frac{(1-2\nu)}{2} & 0 & 0 \\ 0 & 0 & 0 & 0 & \frac{(1-2\nu)}{2} & 0 \\ 0 & 0 & 0 & 0 & 0 & \beta_i \frac{(1-2\nu)}{2} \end{bmatrix} \quad (22)$$

where the superscript ck signifies that the stress-strain relations refer to a coordinate system parallel to principal stress directions with the x^{ck} axis perpendicular to the crack face. If the crack closes, then all compressive stresses normal to the crack plane are transmitted across the crack and only a shear strength reduction factor β_c for a closed crack is introduced. Then $[D_c^{ck}]$ can be expressed as

$$[D_c^{ck}] = \frac{E_c}{(1 + \nu)(1 - 2\nu)} \begin{bmatrix} (1 - \nu) & \nu & \nu & 0 & 0 & 0 \\ \nu & (1 - \nu) & \nu & 0 & 0 & 0 \\ \nu & \nu & (1 - \nu) & 0 & 0 & 0 \\ 0 & 0 & 0 & \beta_c \frac{(1 - 2\nu)}{2} & 0 & 0 \\ 0 & 0 & 0 & 0 & \frac{(1 - 2\nu)}{2} & 0 \\ 0 & 0 & 0 & 0 & 0 & \beta_c \frac{(1 - 2\nu)}{2} \end{bmatrix} \quad (23)$$

The stress-strain relation for concrete that has cracked in two directions are

$$[D_c^{ck}] = E_c \begin{bmatrix} 0 & 0 & 0 & 0 & 0 & 0 \\ 0 & 0 & 0 & 0 & 0 & 0 \\ 0 & 0 & 1 & 0 & 0 & 0 \\ 0 & 0 & 0 & \frac{\beta_t}{2(1 + \nu)} & 0 & 0 \\ 0 & 0 & 0 & 0 & \frac{\beta_t}{2(1 + \nu)} & 0 \\ 0 & 0 & 0 & 0 & 0 & \frac{\beta_t}{2(1 + \nu)} \end{bmatrix} \quad (24)$$

If both directions reclose

$$[D_c^{ck}] = \frac{E_c}{(1 + \nu)(1 - 2\nu)} \begin{bmatrix} (1 - \nu) & \nu & \nu & 0 & 0 & 0 \\ \nu & (1 - \nu) & \nu & 0 & 0 & 0 \\ \nu & \nu & (1 - \nu) & 0 & 0 & 0 \\ 0 & 0 & 0 & \beta_c \frac{(1 - 2\nu)}{2} & 0 & 0 \\ 0 & 0 & 0 & 0 & \beta_c \frac{(1 - 2\nu)}{2} & 0 \\ 0 & 0 & 0 & 0 & 0 & \beta_c \frac{(1 - 2\nu)}{2} \end{bmatrix} \quad (25)$$

The stress-strain relations for concrete that has cracked in all three directions are

$$[D_c^{ck}] = E_c \begin{bmatrix} 0 & 0 & 0 & 0 & 0 & 0 \\ 0 & 0 & 0 & 0 & 0 & 0 \\ 0 & 0 & 0 & 0 & 0 & 0 \\ 0 & 0 & 0 & \frac{\beta_t}{2(1+\nu)} & 0 & 0 \\ 0 & 0 & 0 & 0 & \frac{\beta_t}{2(1+\nu)} & 0 \\ 0 & 0 & 0 & 0 & 0 & \frac{\beta_t}{2(1+\nu)} \end{bmatrix} \quad (26)$$

If all three cracks reclose, Eq. (25) is followed. It should be noted that a check is made to ensure $1 > \beta_c > \beta_t > 0$.

If the material at an integration point fails in uniaxial, biaxial, or triaxial compression, the material is assumed to crush at that point. In concrete element, crushing is defined as the complete deterioration of the structural integrity of the material (e.g., material spalling). Under conditions where crushing has occurred, material strength is assumed to have degraded to an extent such that the contribution to the stiffness of an element at the integration point in question can be reduced or ignored.

3.5 Analysis procedure for nonlinear FEM model

A simple test were carried out on standard concrete cylinders (152 mm in diameter and 304 mm in length), with different layers of carbon fiber sheets (1, 3 and 5 layers). The unconfined concrete properties were $f'_{co} = 17.17$ MPa, $\epsilon_{co} = 0.002$, $E_c = 20,700$ MPa, and $\nu_0 = 0.2$. The CFRP properties are $E_j = 230.54$ GPa, $f_{ju} = 1,152.67$ MPa, $\epsilon_{ju} = 0.005$, and $t_j = 0.1375$ mm/layer (FAW 250). Fig. 3 shows the typical experimental stress-strain curve (coarse and dotted lines) of confined concrete and

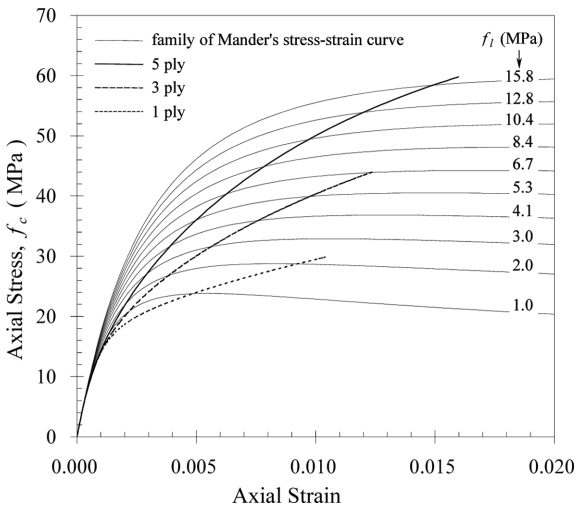


Fig. 3 Typical experimental stress-strain curve of confined concrete

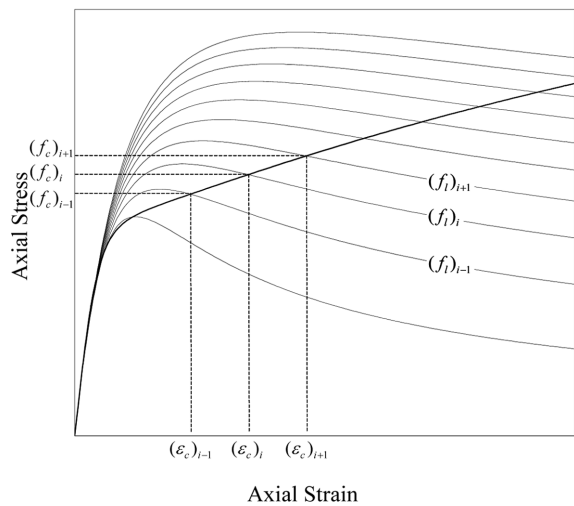


Fig. 4 Nonlinear finite element analysis concept and procedure

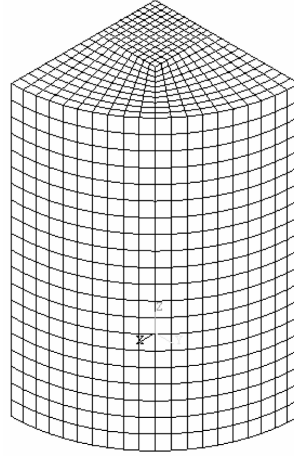


Fig. 5 Element mesh for nonlinear finite element analysis

a family of Mander's curves (fine lines), each one pertaining to a constant level of confining pressure. It can be seen in Fig. 3 that as increasing axial strain all experimental stress-strain curves are passing through the low, medium and high confining pressure of Mander's curves refer to constant confining pressure. It can be proof that the dilation of concrete surrounding by CFRP jacket induced confining pressure is increasing as the axial compressive strain is increasing.

In this paper, the stress-strain characteristics of the confining mechanism are explicitly accounted for, while the lateral strain of concrete is implicitly obtained through the interactive procedure as shown in Fig. 4. The analysis concept can be realized by using commercial computer software, i.e., ABAQUS, ANSYS, MSC/NASTRAN and I-DEAS. In this paper, ABAQUS software (2005) is used and the element meshes of nonlinear finite element model for confined concrete specimens are shown in Fig. 5. The boundary conditions are: $U_x(0, y, z) = 0$ in $x = 0$ plane; $U_y(x, 0, z) = 0$ in $y = 0$ plane; $U_z(x, y, 0) = 0$ in $z = 0$ plane and $U_z(x, y, H/2) = (U_z)_i$ in $z = H/2$ plane corresponding to i step incremental compressive axial strain $(\varepsilon_c)_i$ for displacement control method. The analysis flowchart for nonlinear FEM model is shown in Fig. 6, consists of the following basic steps

1. input column height (H) and column diameter (D)
2. input material properties f'_{co} , ε_{co} , E_c , ν_o for concrete and f_{ju} , ε_{ju} , E_j , ρ_j for CFRP
3. setting compressive axial strain $(\varepsilon_c)_i$ for step i
4. guess confined stress $(f_i^g)_i$, from Eqs. (1), (2) and (5) to find the stress-strain model, and from Eqs. (6) and (9) to form $[D]_{RC}$ and $[D]_{cf}$
5. from commercial FEM software to form nonlinear FEM model and solve composite stress field $\{\sigma\}_{cf}$ and find confining stress $(f_i)_i$
6. check $(f_i^g)_i \cong (f_i)_i$, if $\begin{cases} \text{yes, go to 7} \\ \text{no, adjust } (f_i^g)_i \text{ and repeat 4~6} \end{cases}$
7. solve concrete stress filed $\{\sigma\}_c = [D_c] \{\varepsilon\}_c$ and find compressive axial stress $(f_c)_i$
8. check $\begin{cases} \text{concrete failure occurrence by Willam's criterion, and do stiffness reduction} \\ \text{concrete failure occurrence by Tsai- Wu criterion, and do stop program or not} \end{cases}$
9. next step, incremental strain $(\varepsilon_c)_{i+1}$.

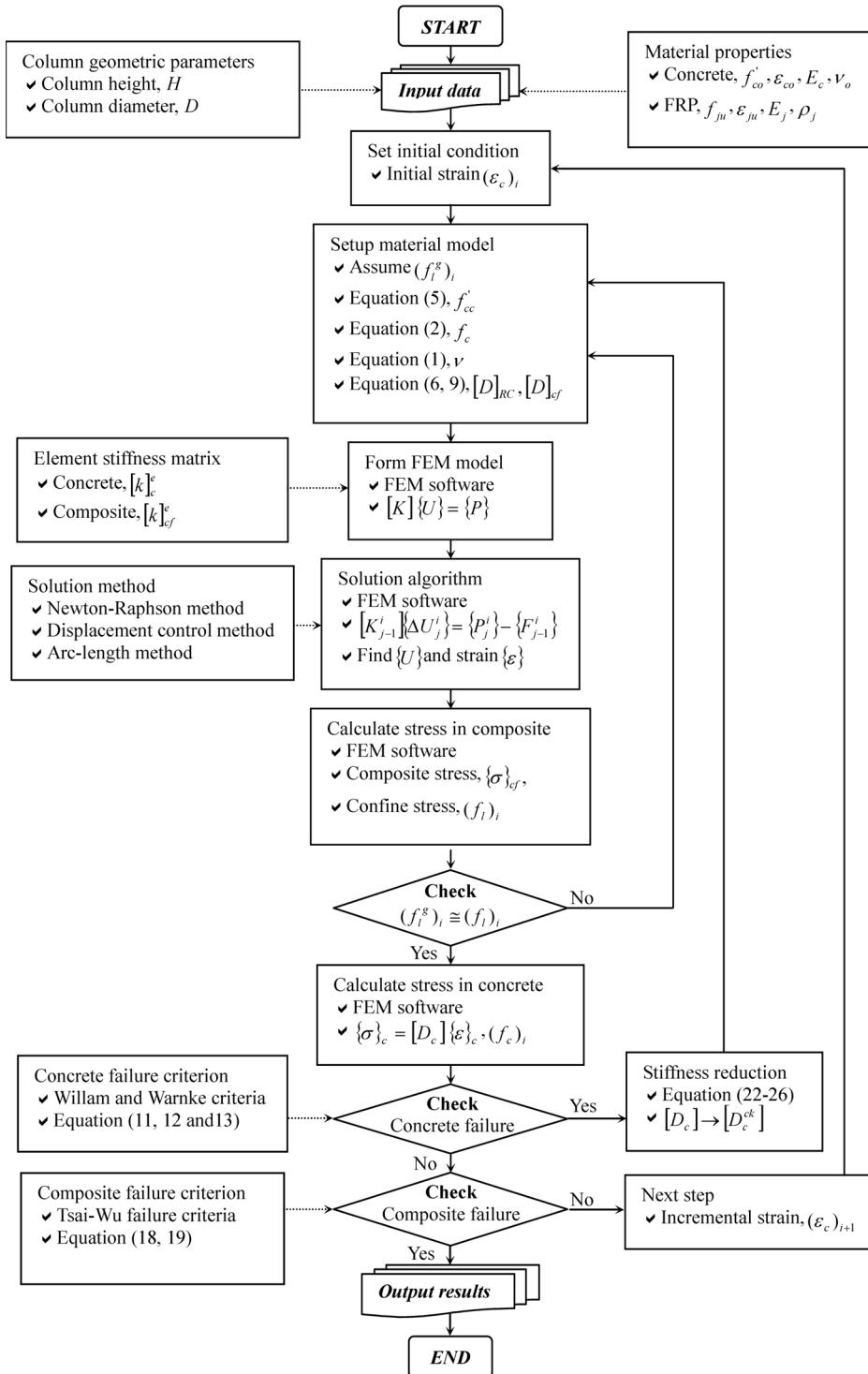


Fig. 6 Analysis flowchart of CFRP confined concrete nonlinear finite element model



Photo 1 Test setup and instrumentation configuration

4. Experimental program

A total of 14 concrete columns with different diameter were constructed and tested under axial compression. The main experimental parameters include column diameter and CFRP volumetric ratio. Table 5 summarized the test matrix. Column diameters (D) considered are 15, 30 and 45 cm. The CFRP volumetric ratios are 0.5, 1.0 and 1.5%.

4.1 Test method and test setup

All the specimens were tested using a high-stiffness, high-capacity (58800 kN) compression testing machine at the Structural Laboratory of Lien-Foo pillar plastic Inc. This unique equipment has sufficient capacity and stiffness, required for conducting such tests. The machine is also equipped with a sophisticated computer control and data acquisition system.

The test procedure was followed the ASTM C39 and CNS 1232 standard and the testing strain rate was 25 micro-strain/sec. The acquired data included the applied axial load, P , axial deformation of concrete, and transverse and axial strain of the FRP jacket. As shown in Photo 1, in order to obtain data without the influence of the possible imperfect contacts and the end confinement due to the friction between the ends of the specimen and the loading platens, the axial deformation of the concrete was measured for the middle portion with a gauge length of $H/2$, using a special device and linear potentiometers. The jacket strains were measured using electrical resistance gauges with a gauge length 10 mm.

4.2 Experimental results

Test results of FRP confined circular concrete columns are shown in Table 5. For columns with 0.55 to 0.59% CFRP volumetric ratio, the maximum compressive strength and ultimate strain are 53.68 MPa and 1.76% (C45-C4-300-2), the minimum compressive strength and ultimate strain are 49.19 MPa and 1.36% (C30-C3-250-1). For columns with 1.03 to 1.1% CFRP volumetric ratio, the

maximum compressive strength and ultimate strain are 72.48 MPa and 2.48% (C30-C5-300-1), the minimum compressive strength and ultimate strain are 66.96 MPa (C45-C7-300-1) and 2.25% (C15-C3-250-1). For columns with 1.47% CFRP volumetric ratio, the maximum compressive strength and ultimate strain are 80.77 MPa and 2.75% (C15-C4-250-1), the minimum compressive strength and ultimate strain are 77.23 MPa and 2.68% (C15-C4-250-2).

Detailed comparisons between experimental results and analysis results are shown in the next section.

5. Comparison with experimental results

5.1 Tests by Picher et al. (1996)

Tests were carried out on five concrete cylinders (152 mm in diameter and 304 mm in length), one unconfined and four confined with different configurations of carbon-fiber sheets. The sheets consisted of three layers wrapped around the concrete specimens with winding angles $[0^{\circ}_3]$, $[0^{\circ}, \pm 6^{\circ}]$, $[0^{\circ}, \pm 12^{\circ}]$, and $[0^{\circ}, \pm 18^{\circ}]$. The unconfined concrete properties were $f'_{co} = 39.7$ MPa, $\varepsilon_{co} = 0.002$, $E_c = 31,500$ MPa, and $\nu_0 = 0.2$.

In order to obtain data without the influence due to the possible imperfect contacts as well as the end confinement due to the friction between the ends of the specimen and the loading plates, the axial deformation of the concrete was measured for the middle portion with a gauge length of half specimen height. The jacket strains were measured using resistance gauges with a gauge length of 30 mm.

Table 2 lists the experimental results and those obtained from the nonlinear FEM analyses. The results show that the absolute errors of compressive strengths for proposed models are 0.00%, 2.86%, 3.51%, 4.34% and 7.95% when specimens are unconfined, C0, C6, C12 and C18, respectively. Also, the results show that the absolute errors of ultimate axial strains for proposed models are 0.00%, 0.93%, 3.41%, 13.59% and 3.03% when specimens are unconfined, C0, C6, C12 and C18, respectively. Fig. 7 shows the comparisons between tests and analyses for the axial stress versus axial strain. As it can be seen in Table 2 and Fig. 7, the agreement between nonlinear finite element results (solid lines) and experimental results (markers) is very satisfactory.

Table 2 Comparisons between tests (Picher et al. 1996) and results of nonlinear finite element model

Specimen	Dimension of section (mm)	f'_{cc} (MPa) (Experiment)	f'_{cc} (MPa) (NFEM)	Error (%)	ε_{cu} (%) (Experiment)	ε_{cu} (%) (NFEM)	Error (%)
Unconfined	152 × 304	39.70	39.70	0.00	0.20	0.20	0.00
C0	152 × 304	55.98	57.58	2.86	1.07	1.08	0.93
C6	152 × 304	52.41	54.25	3.51	0.88	0.91	3.41
C12	152 × 304	49.23	51.37	4.34	1.03	0.89	-13.59
C18	152 × 304	46.05	49.71	7.95	0.66	0.68	3.03

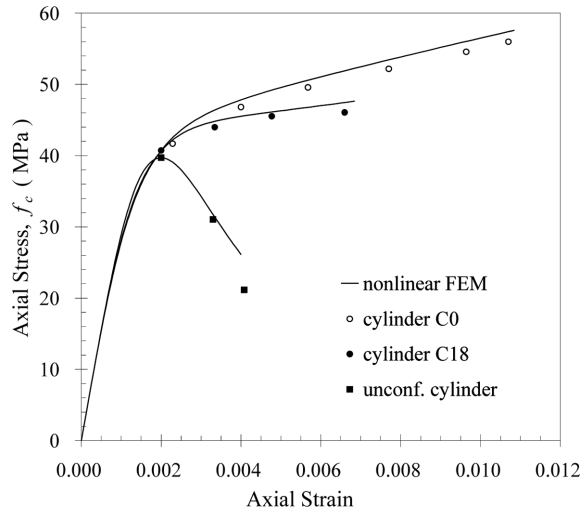


Fig. 7 Comparisons between tests (Picher *et al.* 1996) and analyses for axial stress versus axial strain

5.2 Tests by Kawashima *et al.* (1997)

Kawashima *et al.* (1997) performed a set of experiments on circular reinforced concrete specimens (200 mm in diameter and 600 mm in length) confined with carbon-fiber sheet jackets with different elastic modulus and volumetric jacket ratios ρ_j ranging from 0.5% to 1.3%. Five tests (S1, S3, S4, H3 and H4) on concrete cylinders wrapped with regular modulus (243 GPa) and high modulus (439 GPa) carbon-fiber sheets are examined here. The average unconfined peak strength was $f'_{co} = 39$ MPa, $\epsilon_{co} = 0.0034$, $E_c = 20,000$ MPa, and $\nu = 0.2$.

Consider the diameter to height ratio of specimens in calculating the strengths of experimental results tested by Kawashima *et al.* and converge the test results from $D/H = 1/3$ to $D/H = 1/2$ by increasing about 8% for the strength in Table 3. A comparison with the experimental results of proposed model, Kawashima Model, Miyauchi Model, Xiao and Wu Model, Li *et al.* Model for confined concrete compressive strength and ultimate axial strain are shown in Tables 3, 4 and Figs. 8, 9.

Table 3 lists the volumetric jacket ratios of the two specimens (H3 and H4), along with the experimental results and those obtained from the different stress-strain model for confined concrete. The results show that the errors of compressive strengths for proposed model are -1.17% and -3.74%,

Table 3 Compressive strength comparisons between tests (Kawashima *et al.* 1997) and results of different confined concrete models

Specimen	D (mm)	ρ_j (%)	f'_{cc} (MPa) (Experiment)	Proposed Model		Kawashima Model		Miyauchi Model		Xiao & Wu Model		Li et al. Model	
				f'_{cc} (MPa)	Error (%)								
H3	200 × 600	0.676	75.7	74.81	-1.17	72.63	-4.05	78.79	4.08	70.46	-6.92	79.17	4.58
H4	200 × 600	1.352	96.9	93.27	-3.74	105.59	8.96	118.59	22.38	103.95	7.27	115.35	19.04

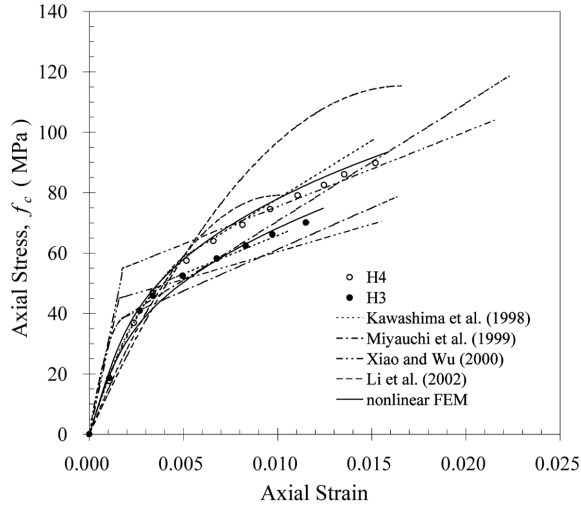


Fig. 8 Comparisons between tests (Kawashima *et al.* 1997) and results of different confined concrete models

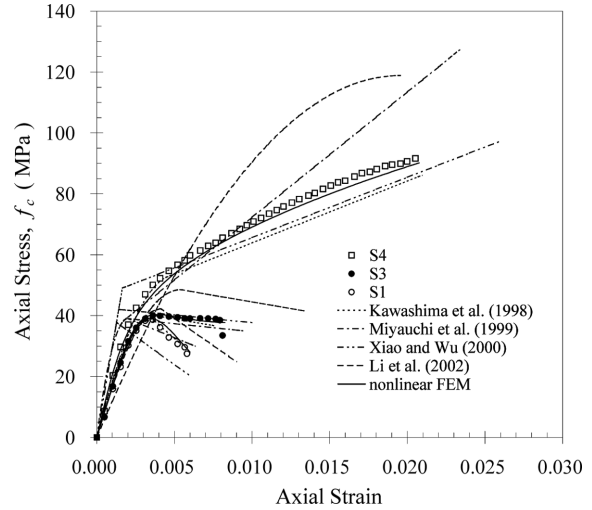


Fig. 9 Comparisons between tests (Kawashima *et al.* 1998) and results of different confined concrete models

Table 4 Ultimate strain comparisons between tests (Kawashima *et al.* 1997) and results of different confined concrete models

Specimen	D (mm)	ρ_f (%)	ε_{cu} (Experiment)	Proposed Model		Kawashima Model		Miyauchi Model		Xiao and Wu Model		Li <i>et al.</i> Model	
				ε_{cu} (%)	Error (%)								
H3	200 × 600	0.676	1.15	1.24	7.83	1.06	-7.83	1.64	42.61	1.55	34.78	1.01	-12.17
H4	200 × 600	1.352	1.52	1.58	3.95	1.52	0.0	2.23	46.71	2.15	41.45	1.67	9.87

for Kawashima Model are -4.05% and 8.96%, for Miyauchi Model are 4.08% and 22.38%, for Xiao & Wu Model are -6.92% and 7.27%, for Li *et al.* Model are 4.58% and 19.04%, respectively. Also, the results show that the errors of ultimate axial strains for proposed model are 7.83% and 3.95%, for Kawashima Model are -7.83% and 0.0%, for Miyauchi Model are 42.61% and 46.71%, for Xiao & Wu Model are 34.78% and 41.45%, for Li *et al.* Model are -12.17% and 9.87%, respectively. Figs. 8 and 9 show the curves for the axial stress versus axial strain obtained from the different FRP confined concrete models. Tables 3, 4 and Figs. 8, 9 show the comparisons between the proposed model and the experimental data, which is extremely satisfactory in term of axial stress versus axial strain.

5.3 Tests by present study - effect of CFRP volumetric ratio

For the columns of fixed plain concrete strength ($f'_{co} = 20.6$ MPa), the effect of CFRP volumetric ratio to the compressive strength and ultimate strain of confined circular concrete columns are shown in Figs. 10 and 11. As shown in Figs. 10 and 11, the normalized compressive strength and ultimate axial strain increase as the CFRP volumetric ratio increase, but not proportion to the CFRP

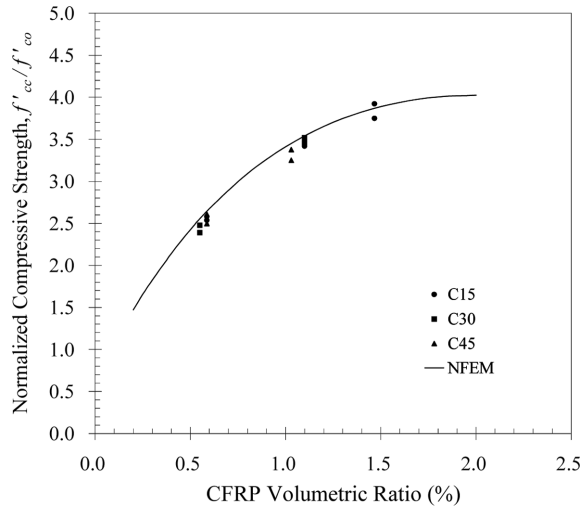


Fig. 10 Comparisons between tests and analyses results for effect of CFRP volumetric ratio on normalized compressive strength

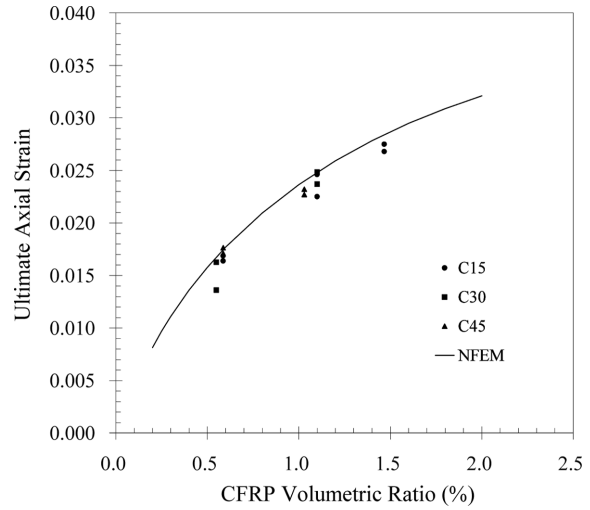


Fig. 11 Comparisons between tests and analyses results for effect of CFRP volumetric ratio on ultimate axial strain

Table 5 Compressive strength comparisons between nonlinear FEM model and test results

Specimen	Dimension of section (mm)	ρ_f (%)	f'_{cc} (MPa)	f'_{cc}/f'_{co} (Experiment)	f'_{cc}/f'_{co} (NFEM)	Error (%)	ϵ_{cu} (%) (Experiment)	ϵ_{cu} (%) (NFEM)	Error (%)
C15-C2-200-1	150 × 300	0.59	53.14	2.58	2.65	2.69	1.69	1.75	3.81
C15-C2-200-2	150 × 300	0.59	52.23	2.54	2.65	4.48	1.64	1.75	6.96
C15-C3-250-1	150 × 300	1.10	70.41	3.42	3.54	3.62	2.25	2.48	10.36
C15-C3-250-2	150 × 300	1.10	71.54	3.47	3.54	1.97	2.46	2.48	0.87
C15-C4-250-1	150 × 300	1.47	80.77	3.92	3.87	-1.29	2.75	2.84	3.42
C15-C4-250-2	150 × 300	1.47	77.23	3.75	3.87	3.25	2.68	2.84	6.16
C30-C3-250-1	300 × 600	0.55	49.19	2.39	2.55	6.84	1.36	1.68	23.25
C30-C3-250-2	300 × 600	0.55	51.04	2.48	2.55	2.97	1.63	1.68	3.11
C30-C5-300-1	300 × 600	1.10	72.48	3.52	3.54	0.66	2.48	2.48	-0.08
C30-C5-300-2	300 × 600	1.10	71.01	3.45	3.54	2.73	2.37	2.48	4.78
C45-C4-300-1	450 × 900	0.59	51.45	2.50	2.65	6.07	1.71	1.75	2.43
C45-C4-300-2	450 × 900	0.59	53.68	2.61	2.65	1.65	1.76	1.75	-0.75
C45-C7-300-1	450 × 900	1.03	66.96	3.25	3.45	6.22	2.27	2.40	5.81
C45-C7-300-2	450 × 900	1.03	69.54	3.38	3.45	2.28	2.32	2.40	3.50

volumetric ratio. As it can be seen in Figs. 10 and 11, the agreements between nonlinear finite element results (solid lines) and experimental results (markers) are quite satisfactory.

5.4 Tests by present study - effect of column size (D)

For the columns of fixed plain concrete strength ($f'_{co} = 20.6$ MPa) and CFRP volumetric ratio

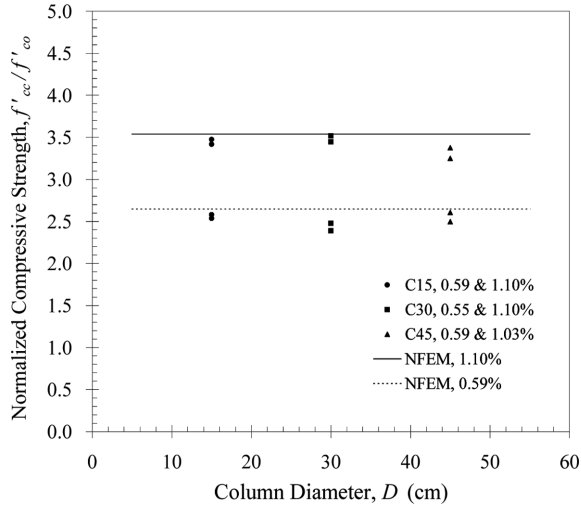


Fig. 12 Comparisons between tests and analyses results for effect of column diameter on normalized compressive strength

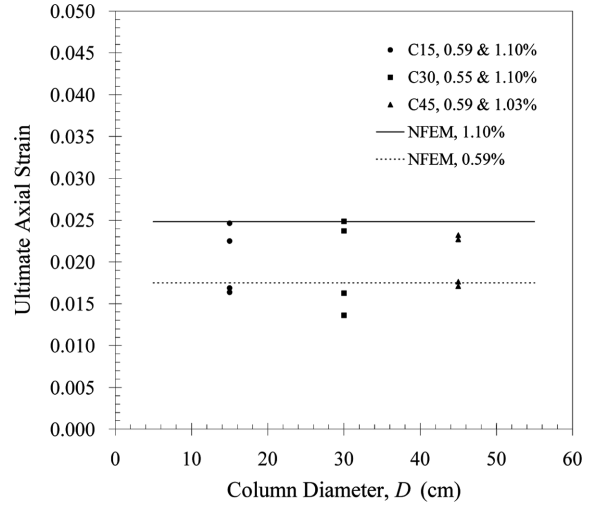


Fig. 13 Comparisons between tests and analyses results for effect of column diameter on ultimate axial strain

(0.5, 1.0%), the effects of column diameter (D) to the compressive strength and ultimate axial strain of the CFRP confined circular concrete columns are shown in Figs. 12 and 13. As shown in these two figure, the normalized compressive strength and ultimate axial strain do not vary with the column diameter, while the CFRP volumetric ratio is fixed to 0.59 and 1.10%. The nonlinear finite element results (solid lines) well predict the experimental results (markers), as shown in Figs. 12 and 13.

6. Parametric study

The parametric study is focused on three factors. They are column diameter, plain concrete strength and reinforcing CFRP volumetric ratio. Consider the plain concrete strength ranging from 6.87 to 34.34 MPa (70 to 350 kgf/cm²), column diameter from 25 to 200 cm, and CFRP volume ratio from 0.0 to 5.0%. The CFRP properties are $E_j = 230.54$ GPa, $f_{ju} = 1,152.67$ MPa, $\varepsilon_{ju} = 0.005$, and $t_j = 0.1375$ mm/layer (FAW 250).

6.1 Classification of FRP confined concrete

It can be seen in Fig. 14 that the different stress-strain curves can be classified into three groups, i.e., Region-I, Region-II and Region III. The characteristic of stress-strain curves in Region-I is including low FRP volumetric ratio, ultimate strength (f'_{cu}) smaller than compressive strength (f'_{cc}) and with descending branch. Nevertheless, the characteristic of stress-strain curves in Region-II is including medium FRP volumetric ratio, ultimate strength (f'_{cu}) greater than compressive strength (f'_{cc}) and without descending branch. The remainders are classified into Region-III.

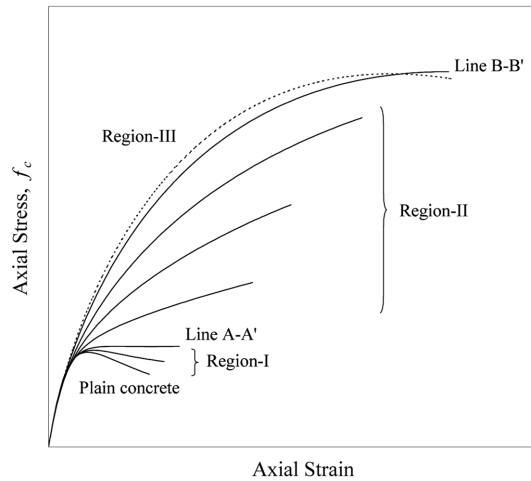


Fig. 14 Classification of stress-strain relations for CFRP confined concrete

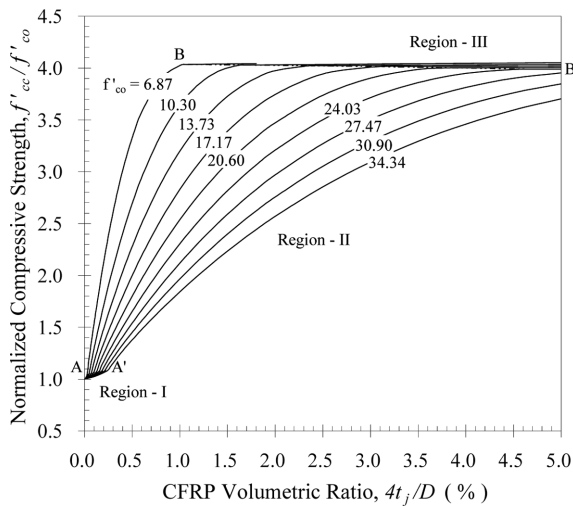


Fig. 15 Relationship of normalized compressive strength and CFRP volumetric ratio

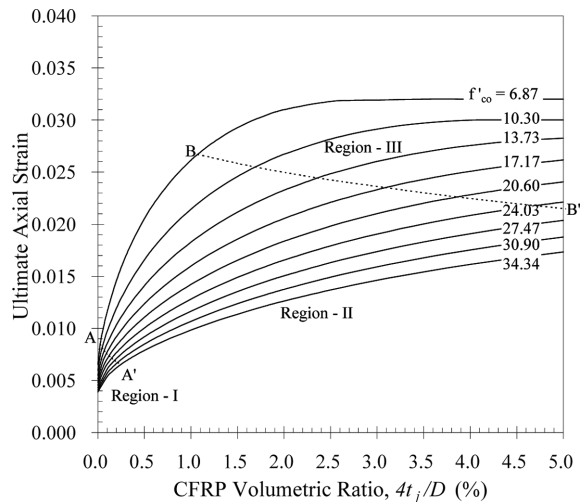


Fig. 16 Relationship of ultimate axial strain and CFRP volumetric ratio

6.2 Effect of CFRP volumetric ratio ($4t_j/D$)

For the columns of fixed plain concrete strength, the influence of changing the CFRP volumetric ratio to the compressive strength and ultimate strain of the confined concrete is studied. Results of parametric study are shown in Figs. 15 and 16. As shown in Fig. 15, for columns with the same plain concrete strength, the normalized compressive strength of confined concrete increases as the CFRP volumetric ratio increases, but not proportion to it. Also, a comparison with confinement efficiency in strength of confined concrete among different regions is shown in Fig. 15. The normalized compressive strength increases slowly in Region-I but increases faster in Region-II. Therefore, the strength confinement efficiency of confined concrete in Region-II is higher than Region-I.

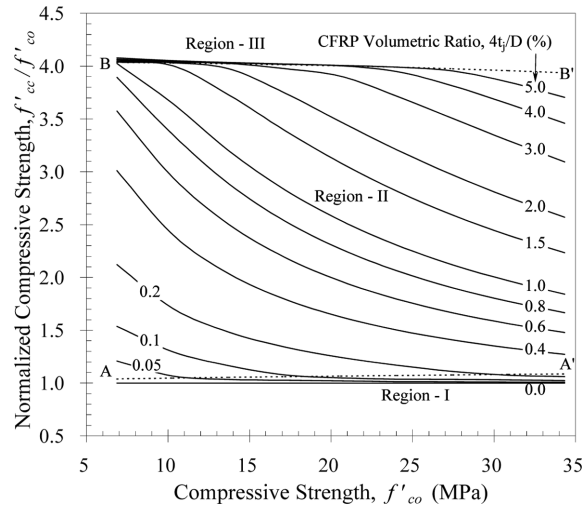


Fig. 17 Relationship of normalized compressive strength and plain concrete strength

As shown in Fig. 16, for columns with the same plain concrete strength, the ultimate axial strain of confined concrete increases as the CFRP volumetric ratio increases, but not proportion to it. Also, a comparison with confinement efficiency in ductility of confined concrete among different regions is shown in Fig. 16. The ultimate axial strain increases fast in Region-I but increases more slowly in Region-II. Therefore, the ductility confinement efficiency in Region-I is higher than Region-II.

6.3 Effect of plain concrete strength

For the columns of fixed CFRP volumetric ratio, the influence of changing the plain concrete strength to the peak compressive strength and ultimate strain of the confined concrete is studied. Results of parametric study are shown in Figs. 17 and 18. As shown in Fig. 17, for columns with the same CFRP volumetric ratio, the normalized compressive strength of confined concrete decreases as the plain concrete strength increases. Also, a comparison with confinement efficiency in strength of confined concrete among different plain concrete strengths is shown in Fig. 17. The strength confinement efficiency of low strength plain concrete is higher than high strength plain concrete, while the columns with the same CFRP volumetric ratio.

As shown in Fig. 18, for columns with the same CFRP volumetric ratio, the ultimate axial strain of confined concrete decreases as the plain concrete strength increases. Also, a comparison with confinement efficiency in ductility of confined concrete among different plain concrete strengths is shown in Fig. 18. The ductility confinement efficiency of low strength plain concrete is higher than high strength plain concrete, while the columns with the same CFRP volumetric ratio.

It is important that the behavior of low strength concrete ($f'_{co} \ll 13.37$ MPa) is somehow not well known and the research only base on the analytical results in this portion, the applications of high confinement efficiency in normalized compressive strength and ultimate axial strain of low strength concrete must be carefully.

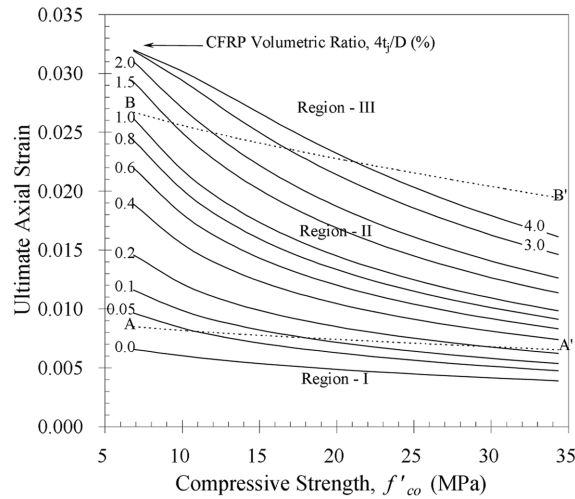


Fig. 18 Relationship of ultimate axial strain and plain concrete strength

6.4 Effect of column size and reinforcing CFRP thickness

For the columns of fixed plain concrete strength, the influence of changing the column diameter and CFRP thickness to the compressive strength and ultimate axial strain of the confined concrete is studied. Results of parametric study are shown in Figs. 19 and 20. As shown in Fig. 19, for columns with the same reinforcing CFRP thickness, the confined concrete strength decreases as the column diameter increases, while the plain concrete strength is fixed to be 27.47 MPa (280 kgf/cm²). However, for columns with the same diameter, the confined concrete strength increases as reinforcing CFRP thickness increases. Nevertheless, the confined concrete strength tends to some

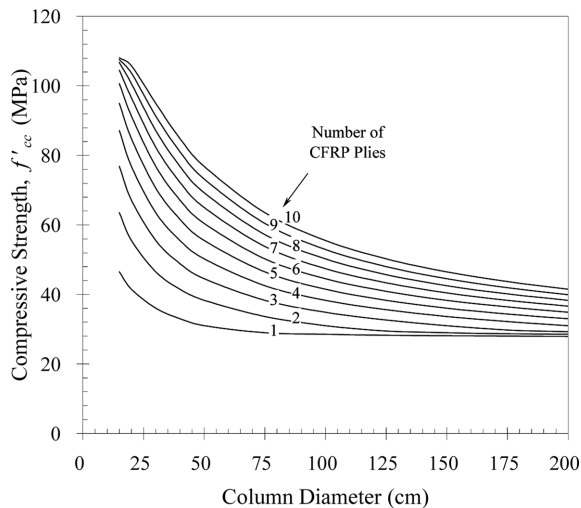


Fig. 19 Compressive strength and column diameter relationship of concrete, $f'_{co} = 27.47$ MPa (280 kgf/cm²)

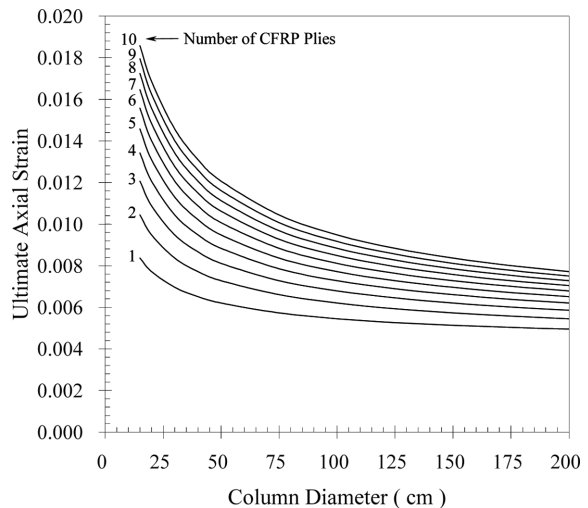


Fig. 20 Ultimate axial strain and column diameter relationship of concrete, $f'_{co} = 27.47$ MPa (280 kgf/cm²)

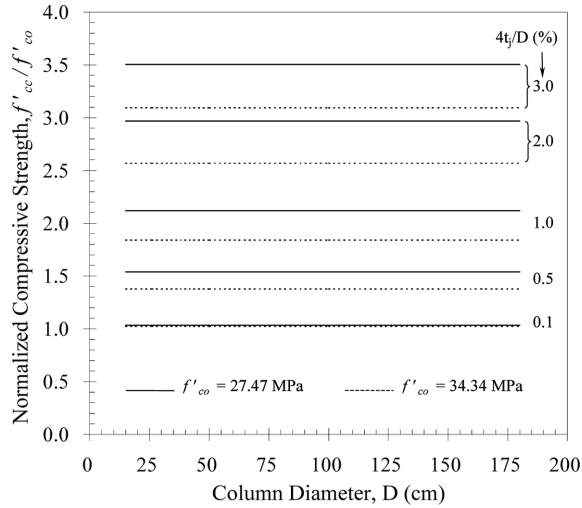


Fig. 21 Relationship of normalized compressive strength and column diameter

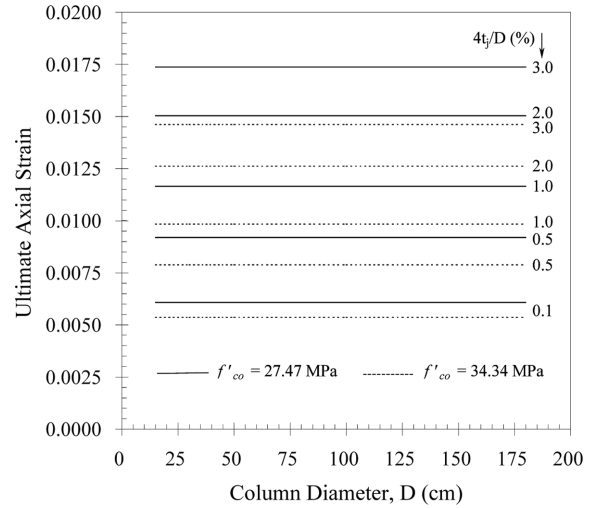


Fig. 22 Relationship of ultimate axial strain and column diameter

certain level for columns with small diameter and thick reinforcing FRP. As the same, the confined concrete strength tends to plain concrete strength level for columns with large diameter and thin reinforcing CFRP.

As shown in Fig. 20, for columns with the same reinforcing CFRP thickness, the confined concrete ductility (ultimate axial strain) decreases as the diameter of column increases, while the plain concrete strength is fixed to be 27.47 MPa (280 kgf/cm²). However, for columns with the same diameter, the confined concrete ductility increases as the reinforcing CFRP thickness of which increases. Nevertheless, the increase of ductility is not proportional to the reinforcing CFRP thickness.

6.5 Effect of column size and FRP volumetric ratio

For the columns of fixed plain concrete strength and CFRP volumetric ratio, the influence of changing the column diameter to the compressive strength and ultimate axial strain of the confined concrete is studied. Results of parametric study are shown in Figs. 21 and 22. As shown in Fig. 21, for columns with the same CFRP volumetric ratio, the normalized compressive strength keep constant and not vary with the column diameter, while the plain concrete strengths are fixed to be 27.47 and 34.34 MPa (280 and 350 kgf/cm²).

Similarly, as shown in Fig. 22, for columns with the same FRP volumetric ratio, the confined concrete ductility (ultimate axial strain) keep constant and not vary with the column diameter, while the plain concrete strengths are fixed to be 27.47 and 34.34 MPa (280 and 350 kgf/cm²). Therefore, there is no size effect, for columns with the same CFRP volumetric ratio but different in diameters.

7. Conclusions

The proposed FRP confined concrete nonlinear finite model, including confined concrete

nonlinear constitutive relation, concrete and composite jacket failure criteria, stiffness reduction methodology and a new analysis procedure, can accurately predict the compressive strength and ultimate axial strain of CFRP confined circular concrete columns.

The effects of changing plain concrete strength, column diameter and CFRP volumetric ratio to strength and ductility of confined circular concrete column are studied by using the nonlinear finite element method. In conclusion, they can be summarized as follows

- (1) The normalized compressive strength and ultimate axial strain of confined circular concrete columns increase as the CFRP volumetric ratio increase, but not proportion to CFRP volumetric ratio, while the columns with the same plain concrete strength before retrofit.
- (2) The strength confinement efficiency of confined circular concrete columns with medium CFRP volumetric ratio (Region-II) are higher than low CFRP volumetric ratio (Region-I). Nevertheless, the ductility confinement efficiency of confined circular concrete columns with low CFRP volumetric ratio (Region-I) is higher than medium CFRP volumetric ratio (Region-II). The behaviors are different from the strength confinement efficiency of confined circular concrete columns.
- (3) The normalized compressive strength and ultimate axial strain of confined circular concrete columns decreases as the plain concrete strength (before retrofit) increases, while the columns with the same CFRP volumetric ratio. Similarly, the strength and ductility confinement efficiency of low strength plain concrete is higher than high strength plain concrete.
- (4) Changing different column diameters while fixing the plain concrete strength (before retrofit) and CFRP volumetric ratio fixed, the normalized compressive strength of circular concrete columns does not vary with the column diameter. In other words, there are no size effects for using CFRP to retrofit circular columns with different diameters, while using the same CFRP volumetric ratio ($4t_f/D$).

Acknowledgements

Results of this study are supported by grants from the National Science Council (NSC 89-2625-Z-002-067).

References

- ABAQUS, Inc. (2005), *ABAQUS Theory Manual and Analysis User's Manual*, Version 6.5, Providence, Rhode Island.
- Fardis, M.N. and Khalili, H. (1982), "FRP-encased concrete as a structural material", *Mag. Concrete Res.*, **34**(122), 191-202.
- Hoshikuma, J., Kawashima, K., Nagaya, K. and Taylor, A.W. (1997), "Stress-strain model for confined reinforced concrete in bridge piers", *J. Struct. Eng.*, ASCE, **123**(5), 624-633.
- Karbhari, V.M. and Gao, Y. (1997), "Composite jacketed concrete under uniaxial compression verification of simple design equations", *J. Mater. Civil Eng.*, ASCE, **9**(4), 185-193.
- Kawashima, K., Hosotani, M. and Hoshikuma, J. (1997), "A model for confinement effect for concrete cylinders confined by carbon fiber sheets", *NCEER-INCEDE Workshop on Earthquake Engrg. Frontiers of Transp. Fac.*, NCEER, State University of New York, Buffalo, N.Y.
- Kupfer, H., Hilsdorf, H.K. and Rusch, H. (1969), "Behavior of concrete under biaxial stresses", *J. Am. Concrete*

- Inst.*, **66**, 656-666.
- Li, Y.F., Lin, C.T. and Sung, Y.Y. (2003), "A constitutive model for concrete confined with carbon fiber reinforced plastics", *Mech. Mater.*, **35**(3-6), 603-619.
- Mander, J.B., Priestley, M.J.N. and Park, R. (1988), "Theoretical stress strain model for confined concrete", *J. Struct. Eng.*, ASCE, **114**(8), 1804-1826.
- Miyauchi, K., Inoue, S., Kuroda, T. and Kobayashi, A. (1999), "Strengthening effects of concrete columns with carbon fiber sheet", *Transactions Japan Concrete Inst.*, **114**, 143-150.
- Picher, F., Rochette, P. and Labossiere, P. (1996), "Confinement of concrete cylinders with CFRP", *Proc., First Int. Conf. on Composites Infrastructures*, Tucson, Ariz., 829-841.
- Popovics, S. (1973), "A numerical approach to the complete stress-strain curves for concrete", *Cement Concrete Res.*, **3**(5), 583-599.
- Saafi, M., Toutanji, H.A. and Li, Z. (1999), "Behavior of concrete column confined with fiber reinforced polymer tubes", *ACI Mater. J.*, ASCE, **96**(4), 500-509.
- Samaan, M., Mirmiran, A. and Shahawy, M. (1998), "Model of concrete confined with fiber composite", *J. Struct. Eng.*, ASCE, **124**(9), 1025-1031.
- Spoelstra, M.R. and Monti, G. (1999), "FRP-confined concrete model", *J. Compos. Constr.*, ASCE, **3**(3), 143-150.
- Toutanji, H.A. (1999), "Stress-strain characteristics of concrete columns externally confined with advanced fiber composite sheets", *ACI Mater. J.*, **96**(3), 397-404.
- Tsai, Stephen W. and Hahn, H.T. (1980), *Introduction to Composite Materials*, Section 7.2, Technomic Publishing Company.
- Tsai, Stephen W. (1987), *Composites Design*, Third Edition, Section 11.6, Think Composites, Dayton, Ohio.
- Willam, K.J. and Warnke, E.P. (1975), "Constitutive model for the triaxial behavior of concrete", *Int. Assoc. Bridge Struct. Eng. Proc.*, **19**, 1-30.
- Xiao, Y. and Wu, H. (2000), "Compressive behavior of concrete confined by carbon fiber composite jackets", *J. Mater. Civil Eng.*, ASCE, **12**(2), 139-146.
- Yuan, X.F., Lam, L. and Smith, S.T. (2001), "FRP-confined RC columns under combined bending and compression: A comparative study of concrete stress-strain models", *FRP Compos. Civil Eng.*, **1**, 749-758.
- Yunus, S.M. and Kohnke, P.C. (1989), "An efficient through-thickness integration scheme in an unlimited layer doubly curved isoparametric composite shell element", *Int. J. Numer. Meth. Eng.*, **28**, 2777-2793.